Journal of Molecular Liquids 438 (2025) 128690

Contents lists available at ScienceDirect

Journal of Molecular Liquids

journal homepage: www.elsevier.com/locate/molliq

Characterisation and application of charcoal-based nanofluids in enhanced oil recovery (EOR)

Hozaifa N. Mohammed [a], Qingchun Yuan [a,b,*], Daniel J. Nowakowski [a,b]

[a] Chemical Engineering and Biotechnologies, School of Engineering and Innovation, College of Physical Science and Engineer, Aston University, Birmingham B7 4ET, United Kingdom

[b] Energy and Bioproduct Research Institute, Aston University, Birmingham B7 4ET, United Kingdom

ARTICLE INFO

Keywords:
Charcoal-based nanofluids
Viscosity enhancement
Enhanced oil recovery
Sectional flooding
Sustainability

ABSTRACT

This study investigates charcoal-based nanofluids for enhanced oil recovery (EOR), as a new route of carbon capture, utilisation and sequestration, contributing to alleviating global warming. Previous studies have shown that the microporous structure of nanoparticles enhance the viscosity of a base fluid better than the counterpart of non-porous ones. A pinewood char with a specific surface area of 107 m^2/g was selected to examine its viscosity enhancement in aqueous suspension and its EOR performance. Pinewood char nanofluids at a nanoparticle size of approximately 155 nm demonstrated a linear viscosity enhancement with charcoal concentration in the range suitable as flooding fluid. Sectional enhanced nanofluid flooding (0.2 pore volume of the core) into sand-packed cores demonstrated that a 0.125 wt% pinewood char nanofluid (viscosity 2.3 mPa•s) achieved 51.4 % recovery of the residue oil in place. The nanofluids demonstrated excellent stability under ambient conditions. These findings highlight the feasibility of using charcoal-based nanofluids as a low-cost, renewable and carbon-negative EOR flooding fluids, offering a possible pathway towards more responsible hydrocarbon production that balances technical performance and environmental impact.

1. Introduction

The oil and gas industry has played a pivotal role in shaping everyday life and global economies for more than a century. In 2023 alone, this sector generated a global revenue of £4.3 trillion (GBP) [1]. Even with increasing use of solar, wind and bio-energies, the oil and gas industry continues to grow at a significant rate as overall energy demand rises. In the UK, for example, 97 % of the energy requirements within the transport sector are met by oil [2]. While oil reserves are estimated to last another 50 years and global energy demand is expected to rise by 50 % by 2050, increasing reservoir complexity continues to challenge conventional recovery methods. These challenges call for cost effective 'zero-carbon' strategies for oil recovery [3].

Oil recovery is commonly classified into primary, secondary and tertiary stages. The primary oil recovery stage uses formation pressure to drive out oil for extraction; the secondary stage normally involves injection of water to top up the reservoir fluid pressure to recover oil. Together these stages recover ~20–40 % of the original oil in place (OOIP), leaving 60–80 % of the OOIP behind due to the reservoir's complexity, e.g., heterogeneous porous rock structure, rock composition, pore and rock distribution of rocks as well as the variation of reservoir fluids [4]. More effective oil recovery is typically pursued at the tertiary stage, also known as enhanced oil recovery (EOR), which involves the injection of specially formulated production fluids that change the flow pattern of reservoir fluids to drive the remaining OOIP to the production well.

The intrinsic heterogeneity of oil reservoirs often leads to the phenomenon of viscous fingering during the second stage of water flooding, where less viscous water bypasses more viscous oil. This eventually results in the formation of "water short paths" from the injection well to the production well, which significantly reduces the recovery efficiency. The formulated production fluids mitigate the viscous fingering via changing their relative mobility to the reservoir fluid towards a uniform displacement of the OOIP. Viscosity, interfacial tension, solubility to the OOIP and wettability to the reservoir rocks are among the fluid properties to be formulated. By manipulating these properties of production fluids according to reservoir conditions and properties, EOR techniques can significantly enhance the volumetric spread of the injected fluids in

* Corresponding author at: Chemical Engineering and Biotechnologies, School of Engineering and Innovation, College of Physical Science and Engineer, Aston University, Birmingham B7 4ET, United Kingdom.

E-mail address: Q.yuan@aston.ac.uk (Q. Yuan).

https://doi.org/10.1016/j.molliq.2025.128690
Received 18 July 2025; Received in revised form 6 September 2025; Accepted 5 October 2025
Available online 9 October 2025

the reservoir, recovering more of the OOIP [5].

Nanofluids leverage unique nanoparticle properties to optimise fluid dynamics within oil reservoirs, notably through viscosity enhancement, wettability alteration, which overall increases EOR performance. Akande et al. reviewed the viscosity enhancement of different metal oxide nanoparticles [6] and systematically studied viscosity enhancement of three charcoal-based nanoparticles [5]. The review disclosed that the viscosity enhancement is strongly influenced by nanoparticle concentration, size/size distribution, shape and agglomeration in the base fluid as well as its interaction to the base fluid (surface chemistry and porosity), which can be collectively described by a parameter of Dispersion Factor. Porous nanoparticles have a higher Dispersion Factor then non-porous ones and enhance viscosity more significantly [5,6]. Youssif et al. [7] studied viscosity enhancement of porous SiO_2 nanoparticles. The porous SiO_2 nanoparticles had a monomodal size distribution, averaged at 22 nm, and a specific area of 370 m^2/g. At a concentration of 0.1 wt%, the nanofluids in 3 wt% of NaCl aqueous solution had a viscosity of 1.16 mPa•s at 20 °C, which is significantly higher than that of water alone.

The study of the charcoal-based nanofluids (charcoals of rice husk, wheat stalk and an active carbon) showed that that charcoal nanoparticles can enhance viscosity more effectively even at much larger particle sizes than metal oxide nanoparticles due to their porosity and surface chemistry [5]. More impressively, the active carbon sample with specific surface area of 1600 m^2/g showed nearly a linear viscosity increase with concentration in the studied range (up to ~5 wt%), comparable to that of multiwall carbon nanotubes when the concentration is lower than <0.6 vol% [8]. When the concentration is higher than 0.6 vol %, the viscosity enhancement of the active carbon surpasses that of the multiple wall carbon nanotube, which levels off due to entanglement of its high aspect ratio of the multiwall carbon nanotube.

The EOR performance study of metal oxide nanofluids such as SiO_2, Al_2O_3, TiO_2 and Fe_2O_3 has demonstrated significant potential. Previous studies have shown that oil recovery initially increases with nanoparticle concentration [7,9,10], reaching optimal performance at certain concentrations (e.g., SiO_2 at 0.1 wt%) [7], yielding an additional recovery of approximately 13 % of the Original Oil in Place (OOIP) compared to conventional water flooding alone. Typically, their EOR performances from sandstone or limestone under different wettability conditions have demonstrated a further oil recovery capacity by 8–16 % of the OOIP after water flooding [7,9,10].

Similarly, charcoal-based nanofluids also showed impressive EOR capabilities [11]. A recent study demonstrated that injecting nanofluids equivalent to 20 % of the pore volume into sandstone-packed cores established a clear correlation between increased nanofluid viscosity and improved oil recovery rates. The oil recovery rate relative to the residual oil in place exceeded 50 %. Notably, the nanofluid of highly porous activated carbon (specific surface area of 1600 m^2/g) demonstrated superior EOR performance, achieving >95 % relative oil recovery, or 34.1 % of the OOIP at a concentration of 2 wt%.

This study aims to further explore the effect of porosity and composition on the viscosity enhancement and the EOR performance of the charcoal-based nanofluids. Samples of a pine wood charcoal (PWC) from biochar processing, which has a significant specific surface area of 107 m^2/g, low ash (1.87 wt%, dry basis) and high carbon (90 wt%, dry basis) contents, and a presentative coconut shell active carbon (CSAC), which has a specific surface area of 1039 m^2/g, were selected for this study.

2. Materials & methods

2.1. Materials

The pine wood char (PWC) sample was provided by the *Urban Biochar and Sustainable Materials Demonstrator* project at Aston University. The sample was pyrolysed at 500 °C with a residence time of 20 min in a Comkiln™ reactor. The coconut shell-based activated carbon (CSAC) used was EcoSorb® DSE-ESCS-A:0707. A colloidal silica nanofluid, obtained from Sigma-Aldrich (Product Number: 420824), was used as a reference. Sand obtained from kiln dried sand (Quartz) was used to pack the cores. Crude oil from Core Laboratories (U·K) Limited, located in Aberdeen, was used. This oil has a measured viscosity of 8.51 mPa•s at room temperature, which sharply decreases with increasing temperature [12].

Synthetic brine was prepared by employing the methodology outlined by Kester et al. [13].

2.2. Nanofluid preparation

The received charcoal particles were firstly ground via a mortar and a pestle to reduce its size to be less than 120 mesh for wet bead milling. Either a planetary micro mill, Pulverisette 7, or Dyno-milling scientific Lab was used to mill with 0.3/0.1 mm zirconium beads in deionised water. The process of wet bead milling proceeded incrementally, commencing with a charcoal concentration of 2.5 wt% of charcoal. Deionised water was used to dilute the fluid for further milling when it became too thick to flow or when particle size reduction plateaued until particle sizes reached the target range. Evaluation of particle size and distribution was conducted through Dynamic Light Scattering (DLS). Prior to DLS analysis, each sample underwent heavy dilution and pH adjustment using either 0.1 M HCl or NaOH aqueous solutions, followed by ultrasonication for 1 h to ensure homogeneity.

2.3. Characterisation of charcoals and nanofluids

2.3.1. Proximate and ultimate analysis

The <120 mesh samples prepared were used for proximate analysis. Each analysis used approximately 3 mg of sample. Proximate analysis was conducted using a Mettler Toledo TGA/DSC2 instrument equipped with STAR^e software. The sample was subjected to a programmed temperature regime in air. Initially, it was heated from 25 to 50 °C at a rate of 15 °C/min, maintained at isothermal conditions for 30 min to eliminate residual moisture. Subsequently, the temperature was increased to 105 °C at a rate of 5 °C/min, followed by another 10-min isothermal hold to ensure complete moisture removal. Further heating from 105 to 750 °C occurred at a rate of 10 °C/min, with a final isothermal hold for 15 min.

A CHNS/O Flash 2000 Organic Elemental Analyser manufactured by Thermo Fisher Scientific was used to determine the elemental composition of the charcoal samples. This includes carbon, hydrogen, nitrogen, sulphur, and oxygen (derived by difference). Each sample, weighing ~3 mg, was combusted along with 4–5 mg of vanadium pentoxide. The gas released was analysed for CO_2, H_2O, NO_2 and SO_2 by the gas chromatography to quantify the content of carbon, hydrogen, nitrogen, and sulphur. The oxygen content was determined by subtracting the sum of C, H, N, S, and ash contents from 100 %. Sulphanilamide served as the standard for the analyses. All reported data represent the average of three measurements, with an average error of 0.7 %.

2.3.2. Fourier transform infra-red (FT-IR)

FTIR spectra were captured using a PerkinElmer Frontier FTIR Spectrometer equipped with the PEAK Technologies GladiATR sampling accessory. Prior to sample measurement, background scans were conducted to mitigate the influence of atmospheric CO_2 and moisture on the spectral background. Each measurement consisted of 16 scans within the range of 4000 to 525 cm^{-1}, at a resolution of 4 cm^{-1}.

2.3.3. pH at the point of zero charge (PZC)

To evaluate the surface charging characteristics of the charcoal, the pH point of zero charge (PZC) was determined for each sample. This parameter denotes the pH value at which the material surface becomes neutral, indicating a zero-charge state. Employing a solid addition method adapted from Liu et al. [14], the PZC of the charcoal samples was assessed. Initial solutions with pH values 1,3,5,7,9 and 11 were prepared using 0.1 M NaOH and HCl aqueous solutions, each in a 12 ml volume. Subsequently, 0.1 g of charcoal samples were dispersed into each solution, followed by placing the samples on a roller (mixer) at 60 rpm for 24 h. The final pH values of the mixtures were recorded, and a plot of final pH against initial pH was drawn to determine the point of zero charge, where initial and final pH values coincide. This was repeated 3 times for each sample. The pH measurements were performed using a Jenway 3540 pH and conductivity meter, calibrated daily with buffer solutions of pH 4.0, 7.0, and 9.2 before each measurement was taken.

2.3.4. BET surface area and pore volume

NOVA 4000e High-Speed Surface Area & Pore Size Analyser manufactured by Quantachrome, equipped with NovaWin™ software, was used to determine the specific surface area and pore volume of the charcoal samples. Prior to gas sorption analysis, samples underwent degassing, which entails removing any surface moisture.

2.3.5. Particle size and size distribution

The charcoal particle size and size distribution of the milled fluid were assessed using Malvern Zetasizer Nano ZSP. The analysis was performed with the measurement angle set to 173° backscatter (default), ensuring optimal characterisation of the charcoal particle size and distribution. The milled fluids were significantly diluted and subjected to ultrasonication after adjusting the pH away from their PZC. A bespoke method was developed, incorporating a 30-s equilibrium time, followed by five runs of 20 s each. Each run comprised five measurements, collectively constituting one measurement cycle. This method has 5 measurement cycles with a 2-s delay between measurements to maintain consistency and accuracy throughout the analysis process.

2.3.6. Viscosity measurement

Viscosity measurements were performed using a Brookfield DV-II Ultra cone rheometer with a CPA-42 spindle. The viscosity measurements were conducted at room temperature with a specified shear rate of 269 s^{-1} (70 rpm). Before measurement, each fluid sample underwent ultrasonication for 1 h at 25 °C to ensure uniformity. The rheometer was calibrated using the viscosity of water at room temperature. To ensure accuracy, each sample was measured at least three times, with reported data having an accuracy within ±0.1 mPa•s.

2.4. Flooding test setup and procedures

2.4.1. Core packing

Cylindrical copper pipes with an inner diameter of 20 mm and a length of 300 mm were used to pack the 'core' with sands ranging from 40 to 60 mesh. To produce a repeatable tightly-packed core, small portions of sand is added each time into the core and then use a metal rod to tap the core for a given time. The porosity of a fully packed core was determined by the pore volume out of the total bed volume by Eq. 1.

$$Porosity\varnothing = \frac{V_P}{V_B} \tag{1}$$

where *Pore Volume* V_p is determined by the weight difference of water saturated core and dry packed core with the specific density of water at 997 kg/m^3; total bed volume V_B is calculated from its cylindrical dimensions.

2.4.2. Oil loading and water flooding

The prepared wet packed core was connected horizontally to the rig assembled in the lab for oil loading and continuous water flooding. A Longer L100-1E peristaltic pump was used to pump the fluid at 2 ml/min. Prior to oil-loading, the packed wet core was rinsed with artificial brine. At the core outlet, a Flomasta pressure reducing valve was installed and adjusted to two turns. At the end of brine rinsing, the back pressure reducer was fully closed, and the core was left under pressure to saturate for 24 h. Subsequently, the core was loaded with oil following the same procedure. During oil loading, effluent was collected in tall thin 25 ml measuring cylinders, and the volumes of both effluent brine and oil were recorded along with the oil pumping time for the creation of oil loading curve. Oil loading stopped when more than 25 ml of oil was collected with no brine observed in the effluent. The total brine volume collected is recorded as that of OOIP. The oil-loaded core was left under pressure to saturate for 24 h before water flooding. The core's temperature was maintained at 50 °C through hot water circulation in the core jacket, regulated by a HAAKE C25P Refrigerated Bath with Phoenix II Controller.

Water flooding was performed under the same conditions as oil loading. Deionised water was pumped in while crude oil in the effluent was monitored. Water flooding concluded when at least 25 ml of water was collected without observable crude oil, after which the core became ready for the EOR test. Each core was subjected to a single flooding sequence ($n = 1$), so the recovery values reported are based on individual runs.

2.4.3. Nanofluid flooding

Sectional flooding of 20 % of the core pore volume was utilised to assess the effectiveness of the nanofluid in enhanced oil recovery. After

Table 1
Proximate and ultimate analysis of the charcoals studied.

	CSAC	PWC
Proximate Analysis (wt% dry basis)		
Ash	5.57	1.87
Organic Matter	94.43	98.13
Ultimate Analysis (wt% dry basis)		
C	83.19	90.12
H	0.81	2.64
N	0.23	0.22
S	0.10	0.00
O (by difference)	10.10	5.15

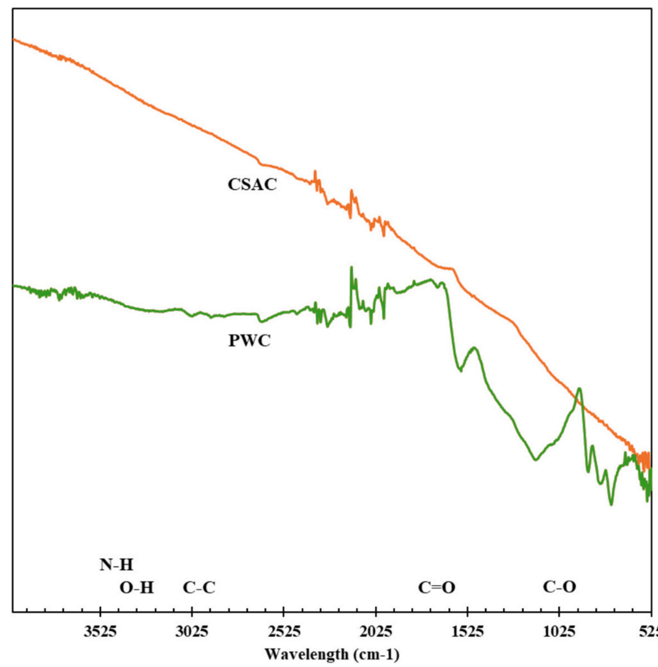

Fig. 1. IR spectra of PWC and CSAC. To understand the surface charge condition of each char in water, the pH point of zero charge was measured.

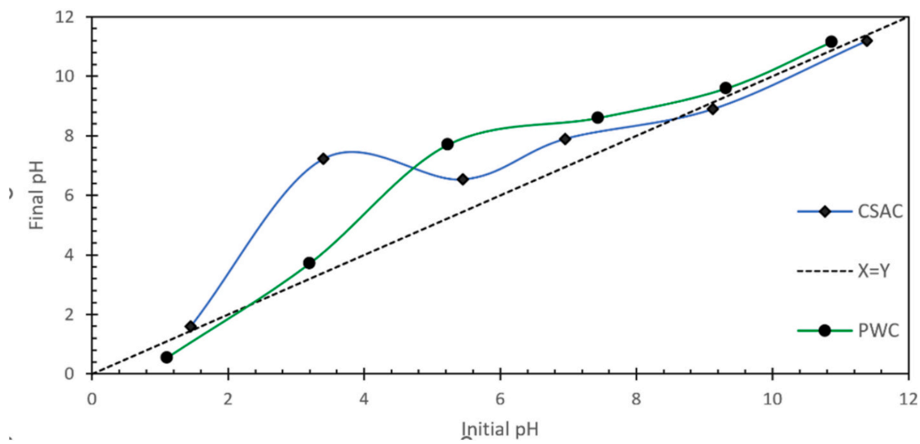

Fig. 2. The final pH value versus corresponding initial pH values for aqueous solutions containing CSAC, PWC. The dotted line represents y = x for finding an accurate PZC value.

the volume of nanofluid injection, water flooding resumed. Throughout this test, crude oil, black nanofluid and creamy-like silica in the effluent were closely monitored and recorded.

3. Results and discussion

3.1. Characterisation of the charcoal samples

The charcoal samples selected were characterised for their proximate and ultimate composition, chemical structure by IR and surface chemistry by determining the pH point of zero charge and porosity. The proximate and ultimate analysis of the PWC and CSAC samples are listed in Table 1. The PWC and CSAC contain 1.87 wt% and 5.57 wt% ash at dry basis, respectively. Both samples are rich in carbon: 90.12 wt% for PWC, 83.19 wt% for CSAC based on dry basis. Their oxygen content is 5.15 wt% for PWC and 10.10 wt% for CSAC.

The chemical structural feature of the charcoal samples was examined by IR. The spectra in Fig. 1 exhibit distinctive differences between the two samples. The CSAC spectrum does not show any significant vibration bond in the wavelength range examined although its oxygen content is nearly twice that of PWC. CSAC shows only faint bands due to its high temperature activation process which strips most oxygen-containing surface groups and leaves a mostly graphitic surface, hence weak bands [15,16] (Fig. 1). In contrast, the PWC has a wide band at ~3225 cm^{-1}, stretching at ~3000–2850 cm^{-1} and at varying peaks at ~1650 cm^{-1}, which corresponds to the O—H vibrations of carboxylic or phenolic groups, aliphatic C—H stretching, and the presence of alkenes or carbonyl groups (aromatic C═C or C═O stretching), respectively. The absorption bands at ~1450–1400 cm^{-1} can be assigned to C—H bending and ~ 1100 cm^{-1} to C—O stretching vibrations.

The spectrum of the PWC shows three sharp vibration bands in the range of 725–925 cm^{-1}. These vibration bands can be assigned to the inorganic ash components of, e.g., calcite, potassium carbonate and magnesite [17], which is consistent with the pine wood ash content like that used as ceramic materials: 41 % CaO, 11 % K_2O and 8 % MgO [18]. The functional groups, elemental compositions, and ash content of charcoals determine their surface chemistry and interactions with the base liquid in the fluid.

The pH point of zero charge (PZC) of the samples were examined to show the surface static- electrical properties. Fig. 2 shows the pH adjustment curves for the two samples, used to determine the pH point of zero charge (PZC). The PZC is identified as the point where the curve intersects the diagonal line, representing equal initial and final pH values after equilibrium during the test.

The PZC readings are pH 2.3 for PWC and pH 8.5 for CSAC. These results show that the zero charge point of the PWC is in a strong acidic range. When the suspension pH value is below 2.3, the surface tends to acquire negative charged ions in environments. When the suspension pH value higher than pH 2.3, the PWC surface is negative tending to acquire positive charged ions. This adsorption increases with pH value to approximately pH 5 and then enters a buff range of ~pH 5 to pH 7.5 at ~pH 8. After this buffing range, the suspension pH turned slightly higher than the original solution.

Table 2
PZC and specific surface area of charcoals studied.

Sample	PZC_{pH}	BET Surface Area (m^2/g)
PWC	2.3	107
CSAC	8.5	1039

The zero charge point of the CSAC located at an alkaline point of pH 8.5. When the suspension pH value is lower than pH 8.5, the surface tends to acquire negatively charged ions in the system with a trend of quick pH value increase up to ~pH 3.5 and reached a kind of plateau in the range of pH 3.5 to pH 8.5. When the suspension pH value higher than pH 8.5, the CSAC surface tends to acquire the positively charged ions. This adsorption results in the suspension pH slightly lower than that of the original solution.

The alkaline surface characteristics observed for CSAC (PZC at pH 8.5) can be attributed to the presence of basic metal oxides in its ash such as potassium oxide (K_2O) [19] which tends to raise the PZC. In contrast, PWC exhibits strongly acidic characteristics (PZC at pH 2.3). Although PWC contains a high proportion of calcite (~41 %) [18], which typically raises the PZC, the low ash content (1.87 wt%) limits its overall influence. As a result, the surface chemistry is dominated by acidic functional groups that significantly lower the PZC. Consequently, CSAC acquires negative surface charges only at relatively alkaline conditions, whereas PWC becomes negatively charged across nearly the entire practical pH range.

The PZC study of the charcoal samples allows the understanding of the dispersion and stability of the nanoparticles in fluids as well as interaction with the reservoir fluids and rocks to be used as flooding fluids for oil recovery. The understanding can be used in the fluid formulation to tailor nanofluid properties to be suitable for specific reservoir conditions.

Table 2 summarises the PZC and specific surface area of the charcoals determined by N_2 gas absorption. CSAC has a larger surface area (1039 m^2/g) than PWC (107 m^2/g).

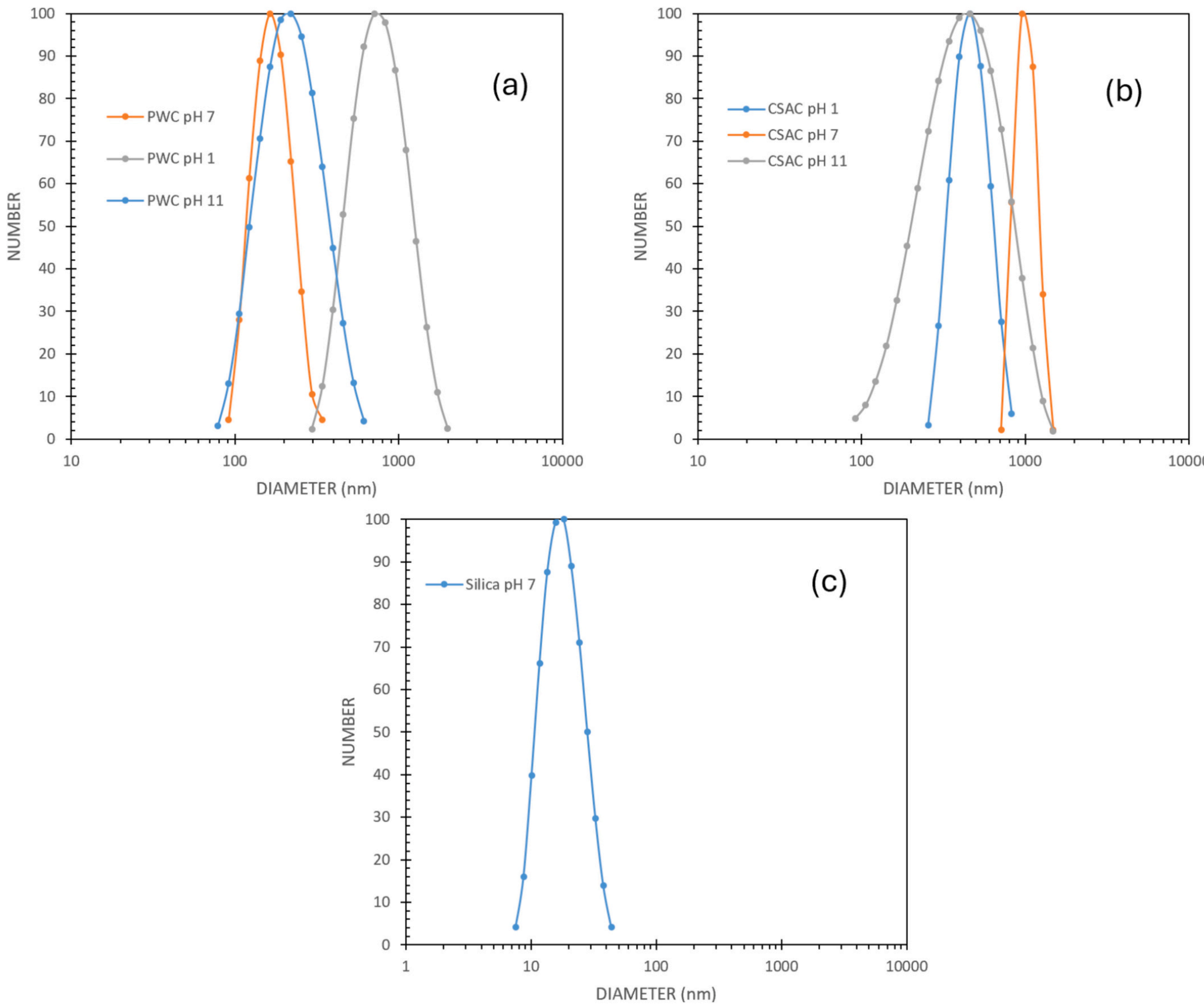

Fig. 3. Effect of pH values on the normalised particle number size distribution of a) PWC, b) CSAC and c) silica nanofluid by Dynamic Light Scattering.

3.2. Nanofluid preparation and characterisation

3.2.1. Nanofluids and particle size characterisation

PWC and CSAC fluids prepared by wet bead milling were observed under a transmission optical microscope with a total magnification of 400×. The charcoal particles of both samples showed adjustable agglomeration by changing the pH condition away from their specific PZC point. After breaking the agglomeration, particles were estimated in the size range of approximately 1 μm in size. The charcoal particles in the nanofluids were further characterised by dynamic light scattering for the particle size and size distribution (see Fig. 3). The measurements conducted at pH 1, pH 7, and pH 11 for each sample showed the effect of pH condition on the measured particle sizes, all of which were below 1 μm.

The PWC sample shows a broad peak centred 712 nm at pH 1, narrower peaks at 164 nm for pH 7, 220 nm for pH 11. As pH moves away from the PZC point of pH 2.3 of PWC sample, the static electronic repulsion between the particles increase. Similarly, the CSAC sample larger particle size of 955 nm at pH 7 (Fig. 3b), which is close to its PZC at pH 8.5. The measured particle size decreases as the pH are adjusted away to pH 1 and pH 11, where the size distribution peaks are 459 nm and 415 nm, respectively. The size distribution peak from the sample at pH 1 is noticeably narrower than that at pH 11, which reflects the difference of pH used for measurement away from the pH of PZC. The particle size distribution peak size (Peak) & half peak width (HPW) are summarised in Table 3. This pH-responsive behaviour in applications like EOR can be used to manipulate the particles to change the fluid microstructure remotely, i.e., inside the reservoir.

Table 3
The particle distribution peak size (Peak) & half peak width (HPW) of the charcoal-based nanofluids.

Sample	pH 1		pH 7		pH 11	
	Peak, nm	HPW, nm	Peak, nm	HPW, nm	Peak, nm	HPW, nm
PWC	712	897	164	120	220	228
CSAC	459	320	955	490	415	660
Silica	–	–	18.2	17	–	–

Adjusting pH away from the PZC effectively reduced particle agglomeration, resulting in smaller particle size distributions (164 nm for PWC at pH 7). This optimal size distribution significantly enhances fluid stability and injectivity, making these nanofluids suitable for sandstone and limestone reservoirs.

Table 4
Viscosities (mPa•s) measurements of the nanofluids at 22 °C.

	2.5 wt%[a]			1.25 wt %[a]	0.5 wt %[b]	0.25 wt %[b]	0.125 wt %[b]
	pH 1	pH 7	pH 11	pH 7	pH 7	pH 7	pH 7
Silica	1.4	–	1.8				
CSAC	3.7	–	7.9	–	–	–	–
PWC	–	117.2	–	53.0	4.5	2.7	2.3

[a] Taken at 70 rpm (269 s^{-1}).
[b] Taken at 100 rpm (384 s^{-1}) and particle average size 155 nm.

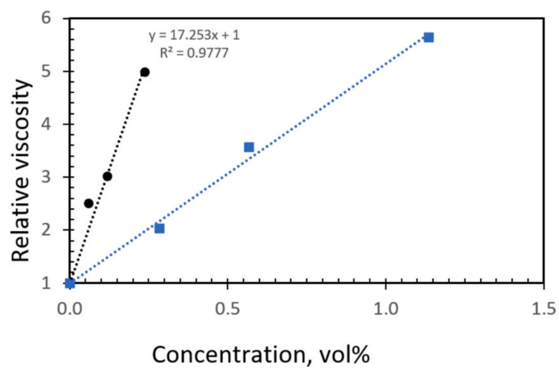

Fig. 4. Relative viscosity of nanofluids versus nanoparticle volumetric fraction: PWC nanoparticles of ~155 nm (black circles), Active carbon of ~250 nm (blue square) [11]. Measured at pH 7, 100 rpm and 22 °C. (For interpretation of the references to colour in this figure legend, the reader is referred to the web version of this article.)

3.2.2. *Viscosity enhancement of the nanofluids*

Previous study showed that concentration and pH values are important parameters to enhance the viscosity of charcoal-based nanofluids [5,7]. The prepared nanofluids of PWC and CSAC were subjected to viscosity measurement at pH values away from their PZCs, namely, pH 1 and pH 11 for the CSAC nanofluids and pH 7 for the PWC nanofluids at varied concentration as listed in Table 4. The viscosity of CSAC nanofluids as prepared at 2.5 wt% is 3.7 mPa•s at pH 1, and 7.9 mPa•s at pH 11. The viscosity enhancement variation with the pH values reflects nanoparticle structure difference in the fluids. At pH 11, the peaked size of 415 nm is slightly smaller than that of 459 nm at pH 1, but the half peak width of nanoparticles of 660 nm at pH 11 is more than double of 320 nm at pH 1, suggesting that more complex microstructure formed from the same CSAC nanoparticles, which gave rise of a strong resistance to the shear force involved in the viscosity measurement and therefore a higher viscosity enhancement.

The viscosity of the PWC nanofluids were measured at the concentrations of 2.5 wt%, 1.25 wt%, 0.5 wt%, 0.25 wt% and 0.125 wt% at pH 7, and showed significant viscosity enhancement with values of 117.2 mPa•s (at 70 rpm), 53.0 mPa•s (at 70 rpm), 4.50 mPa•s (at 100 rpm), 2.72, mPa•s (at 100 rpm), 2.27 mPa•s (at 100 rpm). The values measured at 100 rpm were converted into relative viscosity and plotted against the volume concentration of the nanofluids in Fig. 4. Relative Viscosity = 17.25 x Vol% +1 (R^2 = 0.9777). Comparing with that obtained from another active carbon tested at the same conditions as shown in Fig. 4 [5], we can conclude that the PWC nanoparticles shows stronger viscosity enhancement, and the enhancement is 4.2 times greater than that of AC as reported in [5], and also that of multiwall carbon nanotubes [8]. The impressive viscosity enhancement can be assigned to the following factors:

(1) The microporous structure of the charcoal and the three dimensional nanosized characteristics of the ~155 nm nanoparticles prepared. This size is significantly smaller than ~250 nm reported in [5]. Further reduction in size is expected to enhance the viscosity further.
(2) The chemical composition of the PWC. Fig. 1 suggests PWC contains a significant amount of oxygen-containing functional groups of C═O and —C—O and detectable double valent metal compounds such as Ca^{2+} and Mg^{2+} in the form of calcite and magnesite, for example. Their oxides can account for up to 0.9–1.0 wt% of the PWC. Their existence together with the rich O-containing functional groups may promote particle interaction to the base fluid and to itself for stronger viscosity enhancement.

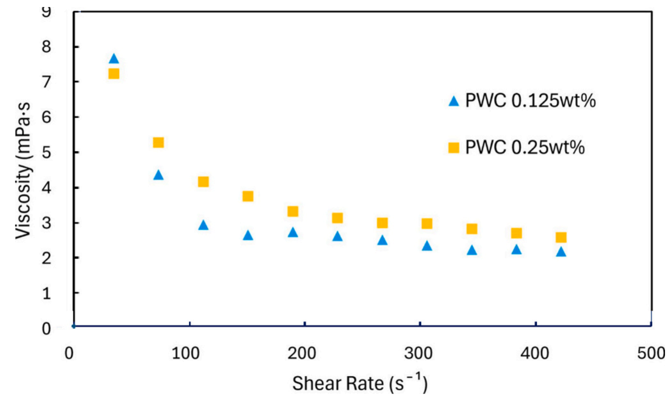

Fig. 5. Viscosity of PWC nanofluids (0.125 wt% and 0.25 wt%) at different shear rates. Taken at pH 7 and at 22 °C temperature.

Rheological analysis (see Fig. 5) demonstrates shear-thinning behaviour in the prepared PWC nanofluids. At a lower shear rate, e.g. 38 s^{-1} viscosity values were notably higher (~7.5 mPa•s for 0.25 wt% and ~ 7.0 mPa•s for 0.125 wt% PWC nanfluids). These values decrease to ~2.5–3.0 mPa•s at shear rates of >300 s^{-1}. In Section 3.2.1 through pH-dependent particle size shifts and microscopic observation suggested microstructure formation in the nanofluids. The observed shear-thinning behaviour further supports their presence where they become disrupted when subjected to increased shear stress thereby reducing flow resistance and viscosity.

The observed shear-thinning property is particularly advantageous for enhanced oil recovery (EOR) applications. High viscosity at lower shear rates could facilitate better mobility control and efficient oil displacement within reservoir pores. Lower viscosity at higher shear rates significantly enhances fluid injectivity which reduces the risk of high injection pressures and formation damage. The rheological profiles reported here align well with previously published findings on carbonaceous nanofluids which confirm the role of particle morphology and surface chemistry in modulating shear-dependent fluid behaviour [11]. Future studies employing microscopic visualisation or scattering techniques could further validate these inferred microstructural dynamics.

Fig. 5 shows both 0.125 wt% and 0.25 wt% which exhibit very similar viscosity profiles at shear rates typical of reservoir injection conditions (>150 s^{-1}). Given the nearly identical viscosity enhancement, the lower concentration (0.125 wt%) was selected as optimal for further evaluation. This choice reduces material usage while maintaining the desired rheological properties necessary for effective EOR applications.

3.3. *Performance of the nanofluids in EOR*

3.3.1. *Core preparation for EOR*

Sandstone packed cores were prepared for the nanofluid performance in enhanced oil recovery. The packed cores were measured for their porosity using the water wetting method and then loaded with crude oil for the volume of original oil in place. Such loaded oil in place

Table 5
Properties of the packed cores for enhanced oil recovery.

Core No.	Porosity, %	Pore volume, ml	Loaded oil, ml	Oil recovered by water flooding, ml
Core #1	27.19	25.63	16.50 (8 min *)	8.70
Core #2	30.44	28.69	26.00 (13 min*)	15.05
Core #3	28.40	26.85	14.50 (5 min *)	6.90
Core #4	31.04	29.26	21.70	14.60
Core #5	31.69	29.87	21.50	11.00

* Oil breakthrough time.

was then subjected to water flooding. Table 5 summaries these properties of the five cores used in this study.

3.3.2. *Nanofluid flooding for EOR*

Nanofluid flooding was carried out by injecting 20 % of the core's pore volume of a nanofluid into the water-flooded cores, followed by water injection at an equivalent pH to that of the nanofluid for enhanced oil recovery. Core #1 was subject to flooding with a 2.5 wt% silica nanofluid (as reference), Core #2 with a 2.5 wt% CSAC nanofluid (at pH 1), and Cores #3, #4 and #5 were used for the flooding of the PWC nanofluids (at pH 7) of 1.25 wt%, 0.5 wt% and 0.125 wt%, respectively.

The Core #1 oil recovery percentage of the original oil in place by water flooding then followed by sectional flooding of 2.5 wt% of silica nanofluids is presented as pore volume ratio (PV, the volume ratio of collected fluid to the pore volume of the core) in Fig. 6.

The oil loaded to Core #1 accounts for 64.4 % of the pore space, i.e.

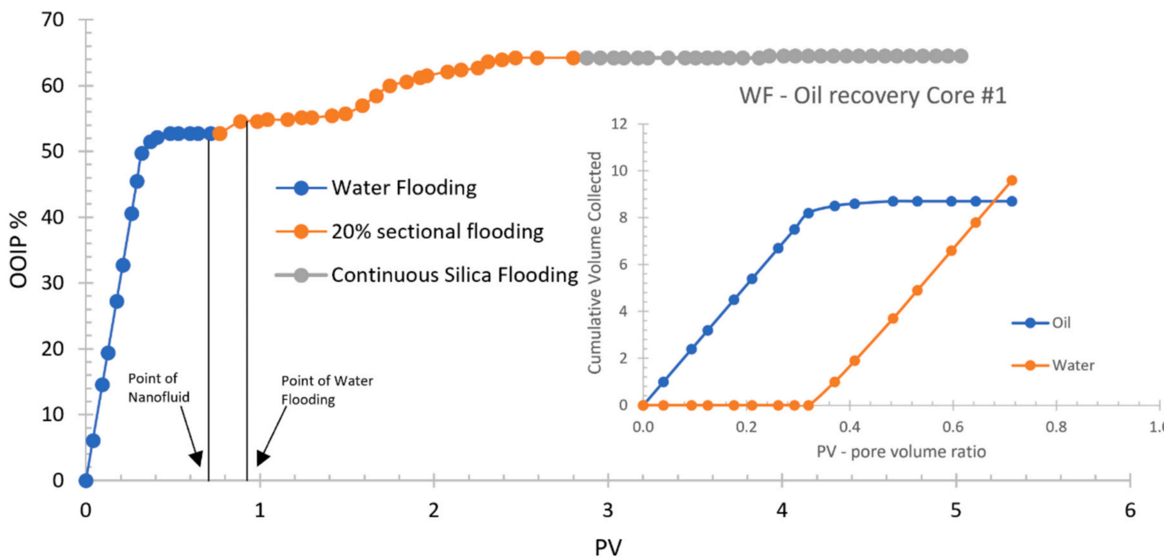

Fig. 6. Core #1: OOIP% vs Pore Volume (ratio of volume collected over pore volume of core). 0.2 PV of 2.5 wt% silica nanofluid injected. The inset shows the oil and water volumes collected during the water flooding.

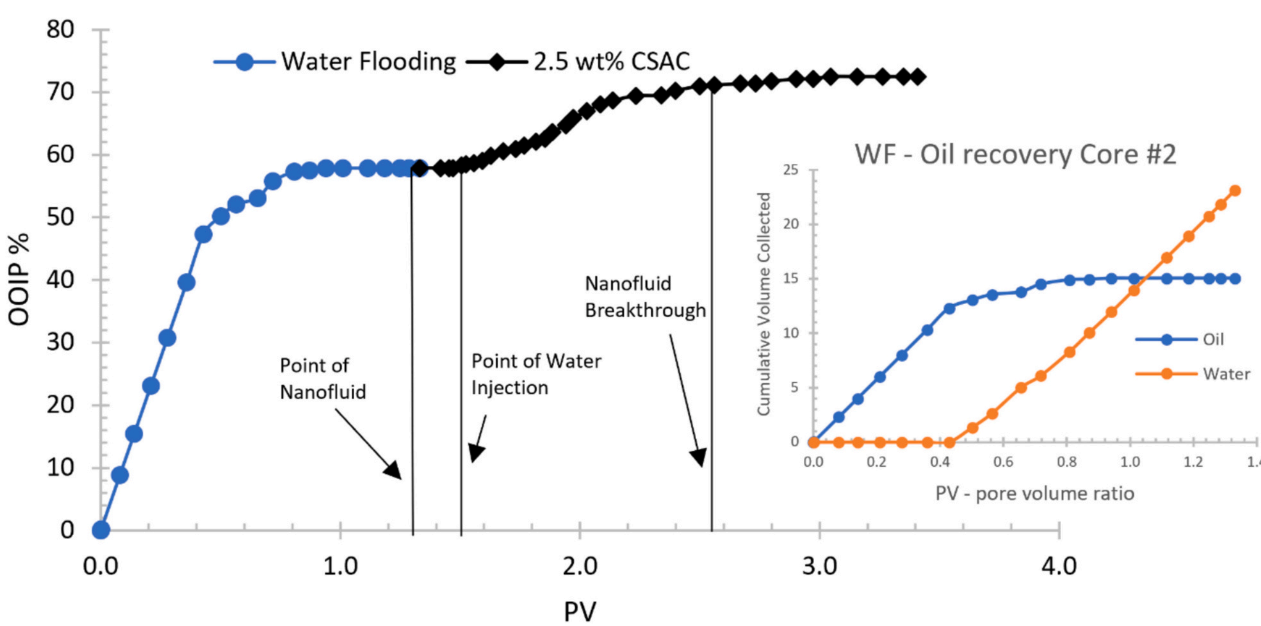

Fig. 7. The recovery of OOIP% vs Pore volume ratio (the ratio of effluent volume collected over the pore volume of core). 0.2 PV CSAC nanofluid injected at pH 1, Core #2.

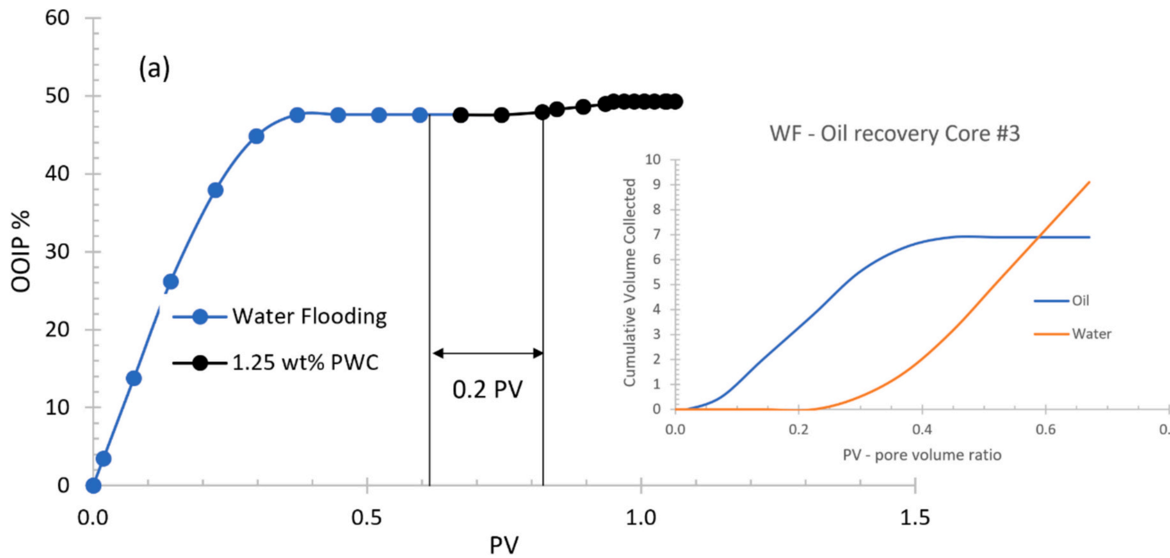

Fig. 8. (a) Core #3: OOIP% vs Pore volume (ratio of volume collected over pore volume of core). 0.2 PV PWC injected. (b) Original oil in place (OOIP) vs time for 2nd trial of 20 % sectional flooding Core #3. (c) 20 % sectional nanofluid of 0.5 wt% PWC Core #4, (d) of 0.125 wt% PWC Core #5.

initial oil saturation. Its water flooding reveals that oil was dominantly recovered by approximately PV = 0.3. At this point water started to appear in the effluent collected, indicating water breakthrough point. As the water flooding continued, water flow shortcuts quickly formed which avoided more oil to be recovered. As a result, the cumulative oil volume reached a plateau shortly at 8.7 ml (52.7 % of the OOIP) at PV = 0.77. Subsequently, 0.2 PV of 2.5 wt% silica nanofluid was injected at a flow rate of 2 ml/min, followed by water flooding at the same flowrate. After the silica nanofluid injection, further water flooding of 2 PV resulted in additional oil being recovered where a total recovery of 64.2 % of the OOIP was achieved. This gives an incremental OOIP recovery of 11.5 %, and 24.3 % of the residual oil in place (ROIP). To evaluate whether the silica nanofluid could extract additional oil, Core #1 was continuously flooded with 2.5 wt% silica fluid at a rate of 2 ml/min for ~2.5 PV (see Fig. 6). The results demonstrated that no additional oil was recovered during this process.

The Core #2 oil recovery profile by water flooding and then sectional flooding of 2.5 wt% CSAC nanofluids is presented in Fig. 7. The Core was loaded by 26 ml of crude oil into its 28.8 ml of porous space, which accounts for 90.3 % of initial oil saturation. During the water flooding, water started to appear at 0.4 PV, which corresponds to a longer time than that of Core #1. The oil recovery of water flooding is levelled at 57.8 % of OOIP at approximately PV = 1.

Sectional flooding of 20 % of the core pore volume with the 2.5 wt% CSAC nanofluid (pH 1) followed by water flooding at the same pH resulted in another significant round of oil recovery (see Fig. 7). The nanofluid injection took place around PV = 1.25, and at PV = 1.6 the recovery rate started to increase significantly, suggesting that the nanofluid took some time to permeate through the pores and displace trapped oil. The point of nanofluid breakthrough was observed at around PV = 2.55. The delayed penetration may be attributed to the higher nanoparticle concentration and large particle size or agglomerates (~459 nm at pH 1) in which the nanofluid became trapped within narrower pore spaces causing partial blockage. This could have led to uneven fluid displacement which promoted some sort of viscous fingering phenomena, wherein portions of the oil were swept by fingering fronts while others remained bypassed. The oil recovery clearly levelled off between PV = 3 and PV = 3.5, resulting in a total recovery of 72.5 % of the OOIP. This represents an enhanced recovery of 14.6 % of the OOIP which corresponds to 34.8 % of the residual oil in place.

The enhanced oil recovery of the 2.5 wt% CSAC nanofluid surpassed that of the 2.5 wt% silica nanofluid by 3.1 %. Its surface charge likely caused repulsion with the charged sand surfaces, which assisted in displacing oil more effectively. This performance is notable and consistent with prior observations in the paper studied by Youssif et al. [7], who reported a recovery of 13.28 % increase of the OOIP with a lower silica concentration of 0.1 wt%, and Alnarabiji et al. [8], who observed a 31.8 % increase in recovery efficiency using multiwall carbon nanotubes below 0.6 vol%. Both studies, however, utilised higher pore volumes for their nanofluid injections compared to the modest 0.2 PV used in this study, underlining the efficiency and cost effectiveness of CSAC sectional nanofluid injection. It is crucial to recognise that variations in core properties also influences these results.

The oil recovery profiles of the Cores #3, #4 and #5 are presented in Figs. 8a-d, respectively, with the 1.25 wt%, 0.5 wt% or 0.125 wt% PWC nanofluids. The oil volume loaded to Core #3 accounts for 54.0 % of its porous space. Its water flooding recovered 47.6 % of the OOIP. During the water flooding, the first drop of water appears at PV = 0.3, and the oil recovery rate levelled at ~PV = 0.65, similar to that of the Core #1. However, the sectional flooding of 1.25 wt% PWC nanofluid and subsequent water flooding through Core #3 encountered a significant pressure increase and resulted in minimal oil displacement and a mostly clear effluent. As shown in Fig. 8a, less than 2 % of the OOIP was recovered in the effluent, which is considered negligible (see Table 6), as this may be attributed to small pressure changes within the core during injection. The excessive viscosity of the nanofluid (53 mPa•s) hindered the fluid's relative mobility preventing it from penetrating the core's pores and blocking its passage through the core. This suggests a critical upper viscosity limit for nanofluid injectivity under the tested conditions. The very high viscosity may be to do with the significant presence of Ca^{2+} and Mg^{2+} ions in PWC contributed to the blockage by influencing particle aggregation.

To address this, a second sectional flooding test on Core #3 was carried out using 1.25 wt% PWC nanofluid at 80 °C, the injection rate of 6 ml/min, and double opening of the back-pressure valve. A nanofluid volume equal to 20 % of the core pore volume (0.2 PV) was directly injected at the upstream end through a syringe needle, followed by waterflooding. A significant volume of oil was gradually recovered, accounting for 41.1 % of the OOIP (Fig. 8b), bringing the total recovery to 90.4 % of the OOIP.

To avoid blockage resulted from highly viscous fluids, the

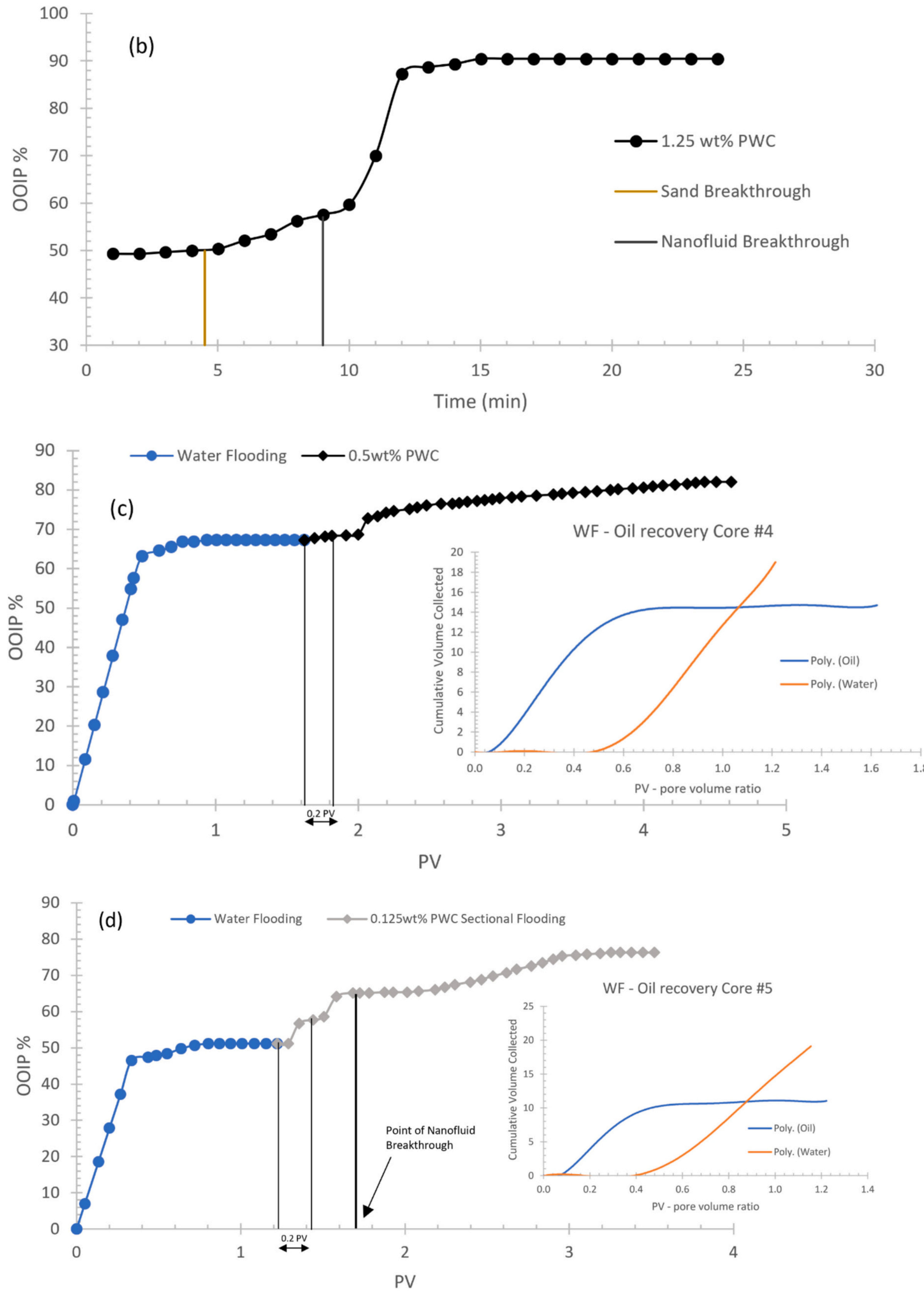

Fig. 8. (*continued*).

concentration of PWC nanofluids was reduced to 0.5 wt% and 0.125 wt % where they were sectionally flooded using Core #4 and #5, respectively. The oil volume loaded into Core #3 and Core #4 was 21.7 ml and 21.5 ml, respectively, which give rise of the initial oil saturation of 74.2 % in Core #4 and 72.0 % in Core #5. The water flooding of Core #4 achieved a recovery rate of 67.3 % of the OOIP, and Core #5 recovered

Table 6
Enhanced oil recovery (EOR) performance of the studied nanofluids.

Sample	Concentration (wt%)	PH	Viscosity (mPa•s)	EOR (OOIP%)
Silica	2.5	7	1.8	11.5
CSAC	2.5	1	3.7	14.6
PWC	1.25	7	53.0	–
PWC	0.5	7	4.5	14.8
PWC	0.125	7	2.3	25.1

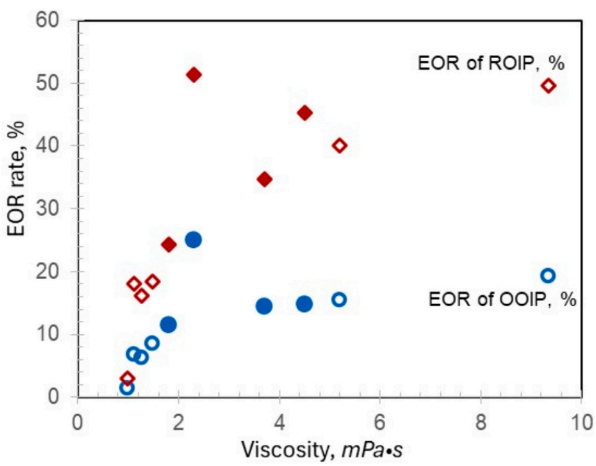

Fig. 9. Enhanced oil recovery rates of the nanofluids versus their viscosities at 22 °C. The cycle points are based on the original oil in place (OOIP) for absolute enhanced oil recovery rate while the rhombus points are relative enhanced oil recovery rate, based on remaining oil in place (ROIP). The Solid points are from this study and the empty ones are from [11].

51.2 % of the OOIP, as shown in Fig. 8b and c, respectively. Both cores demonstrate typical secondary recovery behaviour, where the rate of oil recovery sharply increases early on and then slows down as water breakthrough occurs. Core #4 shows more efficient recovery than core #5 during water flooding. The difference in oil recovery can be attributed to the settling period prior to water flooding discussed previously. Core #4, which had the higher recovery rate, was not left to settle for an extra 24 h. This is because without the extended settling time the oil remains more mobile within the larger pores making it easier to displace during water flooding. Core #5 on the other hand likely experienced increased oil trapping during the additional settling period which led to more oil becoming confined in smaller pore spaces. This reduced the overall recovery efficiency during water flooding. In addition, longer settling times tend to allow capillary forces to trap oil more effectively in the smaller pores, leading to reduced displacement efficiency during water flooding.

Both the 0.5 wt% and 0.125 wt% PWC nanofluid sectional floodings resulted in total oil recovery rates of 82.0 % and 76.3 % of the OOIP, respectively. The nanofluid contributions to these values were 14.8 % OOIP for the 0.5 wt% PWC fluid and 25.1 % OOIP for the 0.125 wt% PWC fluid, corresponding to 45.1 % and 51.4 % of the ROIP, respectively.

For core #4, the 0.5 wt% PWC nanofluid failed to permeate the core completely as no breakthrough was observed. Visual inspection after dismantling the rig showed that the nanofluid had only penetrated approximately halfway through the core. This can be attributed to the fluids relatively high viscosity of 4.5 mPa•s, virtually double the 2.3 mPa•s of the 0.125 wt% PWC nanofluid, which caused reduced fluid mobility and slower but prolonged oil replacement.

Fig. 9 summarises EOR rates versus the nanofluid viscosity. Two EOR rates calculated based on the OOIP and ROIP, respectively, show the absolute oil recovery and relative oil recovery. The latter parameter is used to reduce the effect of oil remaining amount variation after water flooding. EOR rates rise sharply as the viscosity of the 20 % pore volume nanofluids increases from that of water by the viscosity of ~2.3 mPa•s before levelling off. The viscosity of proximately 2.3 mPa•s looks like a transition point, which is given by the 0.125 wt% PWC nanofluid. It may reflect a balance between mobility and injectivity. At lower viscosities, the channelling and viscous fingering left by the previous water flooding is not fully remedied, while above this transient viscosity, the injection pressure increases gradually. On an extreme condition like that observed from Core 3# operation, aggregation and retention of the nanofluid may occur which promotes pore-throat bridging, especially where divalent ions are present (see section 3.2.2). This can cause partial pore blockage and reduce permeability [20–22].

The 20 % sectional floodings of the 0.125 wt% (2.3 mPa•s) and 0.5 wt% (4.5 mPa•s) PWC nanofluids, respectively recovered 25.1 % and 14.8 % of the OOIP. These results outperformed 11.5 % of the OOIP for 2.5 wt% silica (1.8 mPa•s). The silica nanofluid also outperformed the 0.1 wt% silica nanofluids (particle size of 18 nm) reported in the literature [10], which had a recovery of 13.28 % of the OOIP, while multiwall carbon nanotube nanofluids showed an enhanced oil recovery of 31.8 % of the ROIP [8], although both studies utilised much higher pore volumes of the nanofluids. Despite the PWC porous nanoparticles having a size of ~155 nm, its viscosity enhancement at 0.125 wt% surpassed that of the much smaller porous silica nanofluid (specific surface area 370 m^2/g, average size 22 nm) [7]. Similarly, the enhanced oil recovery rate was also higher. The viscosity enhancement is assignable to its nanoscale, porous structure and surface chemistry. The enhanced oil recovery performance of the 0.125 wt% PWC nanofluid supports its potential for cost-effective and sustainable EOR applications. Further reducing the size of PWC may enhance the viscosity further and support its application in EOR.

The 2.5 wt% CSAC nanofluids with its nanoparticles in the size of ~459 nm also showed an impressive enhanced oil recovery rate at 14.6 % of the OOIP or 34.8 % of the residual oil in place, not far from the enhanced oil recovery of 19.1 % of the OOIP or 49.6 % of the ROIP of the 2.0 wt% active carbon nanofluids (particle size at ~210 nm) [11]. Nanofluid stability has been a long-standing challenge as salt ions in the reservoir tend to screen-out the surface charge of the nanoparticles (NPs), rendering them unstable as well as reduced viscosity and interfacial performance [23]. Adding a small amount of surfactants and/or polymers are a popular method to stabilise nanoparticles in the base fluid [24,25]. Notably, the spare charcoal-based nanofluids prepared for flooding has been observed remained uniform after >6 months at ambient conditions by the controlled pH value rather than adding any co-stabiliser. These results demonstrated that charcoal nanoparticle size and concentration can be adjusted together to achieve a desired fluid viscosity to meet different operational requirements. For example, small particle size at lower concentration for the use of low porosity reservoirs, large particle size at a higher concentration for carbon utilisation and sequestration.

4. Conclusion

The charcoal-based nanofluids, namely pinewood char (PWC) nanofluids were prepared for its porosity and composition effect on the viscosity enhancement and the EOR performance. PWC with a specific surface area of 107 m^2/g, low ash (1.87 wt%, dry basis) and high carbon (90 wt%, dry basis) contents was milled down to approximately 155 nm in water. The formed aqueous nanofluids showed shear thinning behaviour and a strong linear viscosity enhancement over 0–1.25 wt%. The viscosity enhancement is 4.2 times greater than that of active carbon [11]. Sectional flooding of PWC at 0.125 wt%, with a viscosity of 2.3 mPa•s, delivered the highest incremental recovery. This outcome significantly surpasses that from silica of this work and porous silica in [7] or carbon nanotube in [8]. The PWC nanofluids used for flooding tests remained stable at ambient conditions for over 6 months which undoubtedly meets the operational requirements. Charcoal-based nanofluids, specifically pine wood char (PWC), offer a promising pathway as a sustainable CCUS (carbon-capture, utilisation and sequestration) method for EOR operation.

CRediT authorship contribution statement

Hozaifa N. Mohammed: Writing – original draft, Project administration, Methodology, Investigation, Formal analysis, Data curation, Conceptualization. **Qingchun Yuan:** Writing – review & editing, Validation, Supervision, Resources, Methodology, Investigation, Funding acquisition, Formal analysis, Data curation, Conceptualization. **Daniel J. Nowakowski:** Writing – review & editing, Resources, Formal analysis.

Declaration of competing interest

The authors declare that they have no known competing financial interests or personal relationships that could have appeared to influence the work reported in this paper.

Acknowledgements

The authors extend their sincere gratitude to the “Urban Biochar and Sustainable Materials Demonstrator” project, funded by the European Regional Development Fund and the local growth fund, in collaboration with Aston University and Combined Industries Ltd., for generously providing us with their biochar samples. Additionally, we acknowledge Aston University for granting access to their invaluable laboratory facilities.

Data availability

No data was used for the research described in the article.

References

[1] Global Oil & Gas Exploration & production - market size, industry analysis, trends and forecasts (2023–2028), IBISWorld, IBISWorld Industry Reports, 2023. https://www.ibisworld.com/global/market-research-reports/global-oil-gas-exploration-production-industry/#Methodology.
[2] UKOG Energy for Britain, UKOG, Accessed on: https://www.ukogplc.com/page.php?pID=74, 2023.
[3] EIA projects nearly 50% increase in world energy usage by 2050, led by growth in Asia, Homepage - U.S. Energy Information Administration (EIA), 2019. https://www.eia.gov/todayinenergy/detail.php?id=41433.
[4] A. Muggeridge, A. Cockin, K. Webb, H. Frampton, I. Collins, T. Moulds, et al., Recovery rates, enhanced oil recovery and technological limits, Philos. Trans. R. Soc. A Math. Phys. Eng. Sci. 372 (2014) 20120320, https://doi.org/10.1098/rsta.2012.0320.
[5] I. Akande, T. Bridgwater, P.J. van Koningsbruggen, Q. Yuan, A viscosity study of charcoal-based nanofluids towards enhanced oil recovery, J. Mol. Liq. 387 (2023) 122615, https://doi.org/10.1016/j.molliq.2023.122615.
[6] I. Akande, T. Bridgwater, P.J. van Koningsbruggen, Q. Yuan, Advances in the modelling of concentration-dependent relative viscosity data for nanofluids by introducing the dispersion factor, J. Mol. Liq. 380 (2023) 121644, https://doi.org/10.1016/j.molliq.2023.121644.
[7] M.I. Youssif, R.M. El-Maghraby, S.M. Saleh, A. Elgibaly, Silica nanofluid flooding for enhanced oil recovery in sandstone rocks, Egypt. J. Pet. 27 (2018) 105–110, https://doi.org/10.1016/j.ejpe.2017.01.006.
[8] M.S. Alnarabiji, N. Yahya, A. Shafie, H. Solemani, K. Chandran, S.B. Hamid, et al., The influence of hydrophobic multiwall carbon nanotubes concentration on enhanced oil recovery, Procedia Eng. 148 (2016) 1137–1140, https://doi.org/10.1016/j.proeng.2016.06.564.
[9] A. Esfandyari Bayat, R. Junin, A. Samsuri, A. Piroozian, M. Hokmabadi, Impact of metal oxide nanoparticles on enhanced oil recovery from limestone media at several temperatures, Energy Fuel 28 (2014) 6255–6266, https://doi.org/10.1021/ef5013616.
[10] N.A. Ogolo, O.A. Olafuyi, M.O. Onyekonwu, Enhanced oil recovery using nanoparticles, All Days (2012), https://doi.org/10.2118/160847-ms.
[11] I.Z. Akande, Development of Charcoal-Based Nanofluids for Enhanced Oil Recovery, Aston University, 2023.
[12] P.V. Hemmingsen, A. Silset, A. Hannisdal, J. Sjöblom, Emulsions of heavy crude oils. I: influence of viscosity, temperature, and dilution, J. Dispers. Sci. Technol. 26 (2005) 615–627, https://doi.org/10.1081/dis-200057671.
[13] D.R. Kester, I.W. Duedall, D.N. Connors, R.M. Pytkowicz, Preparation of artificial seawater1, Limnol. Oceanogr. 12 (1967) 176–179, https://doi.org/10.4319/lo.1967.12.1.0176.
[14] Y. Liu, X. Zhao, J. Li, D. Ma, R. Han, Characterization of bio-char from pyrolysis of wheat straw and its evaluation on methylene blue adsorption, Desalin. Water Treat. 46 (2012) 115–123, https://doi.org/10.1080/19443994.2012.677408.
[15] R. Ali, Z. Aslam, R.A. Shawabkeh, A. Asghar, I.A. Hussein, BET, FTIR, and RAMAN characterizations of activated carbon from waste oil fly ash, Turk. J. Chem. 44 (2) (2020) 279–295, https://doi.org/10.3906/kim-1909-20.
[16] P. Lawtae, C. Tangsathitkulchai, A new approach for controlling mesoporosity in activated carbon by the consecutive process of air oxidation, thermal destruction of surface functional groups, and carbon activation (the OTA method), Molecules 26 (2021) 2758, https://doi.org/10.3390/molecules26092758.
[17] A. Kharchafi, J. Dahmani, K. Tanji, A. El Gaidoumi, E. Iboustaten, Y. Fahoul, M. Belghiti, I. El Mrabet, A. Arrahli, A. Kherbeche, Lizardite’s capacity for carbon dioxide sequestration through a mineral process, React. Kinet. Mech. Catal. 137 (2024) 339–358, https://doi.org/10.1007/s11144-023-02547-0.
[18] J. Dibdiakova, L. Wang, H. Li, Characterization of ashes from Pinus sylvestris forest biomass, Energy Procedia 75 (2015) 186–191, https://doi.org/10.1016/j.egypro.2015.07.289.
[19] S. Aluvihara, C.S. Kalpage, P.W.S.K. Bandaranayake, Manufacturing of activated carbon using disposable coconut shells for catalytic activities and water treatment utilizations, in: Technology transfer: fundamental principles and innovative technical solutions, 2020, https://doi.org/10.21303/2585-6847.2020.001537.
[20] A. Al-Asadi, E. Rodil, A. Soto, Nanoparticles in chemical EOR: a review on flooding tests, Nanomaterials 12 (2022) 4142, https://doi.org/10.3390/nano12234142.
[21] Q. Tong, Z. Fan, Q. Liu, S. Qiao, L. Cai, Y. Fu, X. Zhang, A. Sun, Research progress in nanofluid-enhanced oil recovery technology and mechanism, Molecules 28 (2023) 7478, https://doi.org/10.3390/molecules28227478.
[22] F. Wang, H. Xu, Y. Liu, Y. Jiang, C. Wu, Experimental study on the enhanced oil recovery mechanism of an ordinary heavy oil field by polymer flooding, ACS Omega 8 (2023) 14089–14096, https://doi.org/10.1021/acsomega.2c08084.
[23] N. Lashari, T. Ganat, K.A. Elraies, M.A. Ayoub, S. Kalam, T.A. Chandio, S. Qureshi, T. Sharma, Impact of nanoparticles stability on rheology, interfacial tension, and wettability in chemical enhanced oil recovery: a critical parametric review, J. Pet. Sci. Eng. 212 (2022) 110199, https://doi.org/10.1016/j.petrol.2022.110199.
[24] R.S. Kumar, K.R. Chaturvedi, S. Iglauer, J. Trivedi, T. Sharma, Impact of anionic surfactant on stability, viscoelastic moduli, and oil recovery of silica nanofluid in saline environment, J. Pet. Sci. Eng. 95 (2020) 107634, https://doi.org/10.1016/j.petrol.2020.107634.
[25] T. Sharma, N. Velmurugan, P. Patel, B.H. Chon, J.S. Sangwai, Use of oil-in-water Pickering emulsion stabilized by nanoparticles in combination with polymer flood for enhanced oil recovery, Pet. Sci. Technol. 33 (17–18) (2015), https://doi.org/10.1080/10916466.2015.1079534.